DOI: 10.13009/EUCASS2023-514

Aerospace Europe Conference 2023 – 10TH EUCASS – 9TH CEAS

DOI: ADD DOINUMBER HERE

Combustion Instabilities Induced by Multi-Stepped Hybrid Rocket Fuel Grains

Artur Elias de Morais Bertoldi[1, 2†], Christopher Glaser[3], Jouke Hijlkema[3], Jean-Yves Lestrade[3], Jérôme Anthoine[3], Riccardo Gelain[1] and Patrick Hendrick[1]

[1] Aero-Thermo-Mechanics Department, Université Libre de Bruxelles

50 Avenue F. D. Roosevelt, 1050 Brussels, Belgium.

[2]Chemical Propulsion Laboratory, University of Brasilia

Área Especial de Indústria Projeção A,72444-240, Brasília, Brazil.

[3]ONERA/DMPE, Université de Toulouse

F-31410 Mauzac, France.

artur.elias.de.morais.bertoldi@ulb.be, christopher.glaser@onera.fr, jouke.hijlkema@onera.fr, jean-yves.lestrade@onera.fr, jerome.anthoine@onera.fr, Riccardo.Gelain@ulb.be, patrick.hendrick@ulb.be

[†] Corresponding Author

Abstract

Previous research using Forward Facing Steps (FFS) and Backward Facing Steps (BFS) in the solid fuel grain demonstrated increased regression rates compared to a cylindrical single port. Nonetheless, it is important to assess the combustion instabilities induced by stepped geometries to anticipate (and solve) potential negative side effects. This paper addresses the preliminary experimental results for single and multi-step configurations and their combustion chamber pressure oscillations. Additionally, the impact of a stepped helix approach on the combustion behaviour is assessed. Pressure oscillations in hybrid rockets are not likely to be as limiting compared to their liquid and solid counterparts. However, the instabilities might significantly affect the performance and payload comfort of the propulsive system. In this study, we analyse the interaction between the pressure oscillations in the combustion chamber and the other parameters of the HYCAT (HYbrid with CATalyst) hybrid rocket motor at ONERA. We show that although steps play a major role in pressure oscillations and significantly alter the combustion behaviour of the engine, none of the stepped cases exceeded the most instable no-step test; on the contrary, especially BFSs have the potential to decrease pressure oscillations. This remark is important because multi-stepped grains have significantly higher regression rates (26 % to 245 %) than the cylindrical reference cases.

1. Introduction

The hybrid rocket propulsion system has been considered as a technological option for small satellites launchers, upper stages of launch systems, decelerator engines for re-entry capsules, reusable spacecraft orbit transfer, and new generation transportation systems due to specific qualities such as safety aspects, applications flexibility, grain robustness, and propellant versatility [1,2]. Hybrid Rocket Engines (HREs), in general, have a lower development cost in comparison with liquid rocket engines and safer assets related to transporting and handling when compared to solid rocket motors [3-5]. Still, HREs have some development challenges due to the low regression rate of the solid fuel grain, combustion efficiency and combustion instabilities [6, 7]. The regression rate for commonly employed solid fuels such as Hydroxyl-Terminated Polybutadiene (HTPB) and High-Density Polyethylene (HDPE) is low due to their boundary layer combustion mechanism [8].

The profile of the HRE fuel grain has a considerable impact on the propulsive characteristics of the engine. The simplest grain design is a single cylindrical port. When multiple ports are required to increase the burning surface and, therefore, the fuel mass flow, several problems are introduced, such as pressure differences between the ports. Moreover, a circular shape of each of the multi-ports can lead to high residuals and inefficient volumetric loading. In these situations, sometimes, longer motors are used to increase the burning surface, which creates control problems in flight [4]. On the other hand, changing the geometry from a single circular port to a star shaped grain or swirling ports, for example, can increase the effective burning rates [9, 10]. Various techniques have been applied over the years to

DOI: 10.13009/EUCASS2023-514

increase the solid fuel regression rate and one of the more effective and simpler ones is the changing of the grain configuration to increase mixing and heat transfer [11].
Previous research carried out by the authors using a single *Forward Facing Step* (FFS) or *Backward Facing Step* (BFS) demonstrated increased regression rates for FFS and BFS grains in comparison with a cylindrical single port [12]. The stepped concept proposed first by Glaser et al. [12,13], Figure 1(a), approximates an idealised fuel port by a set of cylinders with different inner fuel diameters, as seen in Figure 1(b). Because of the steps, recirculation zones are induced that increase mixing and heat transfer. This design is easy to manufacture since there is no need for additive manufacturing, which otherwise would be necessary to manufacture the optimised profiles [12,13].

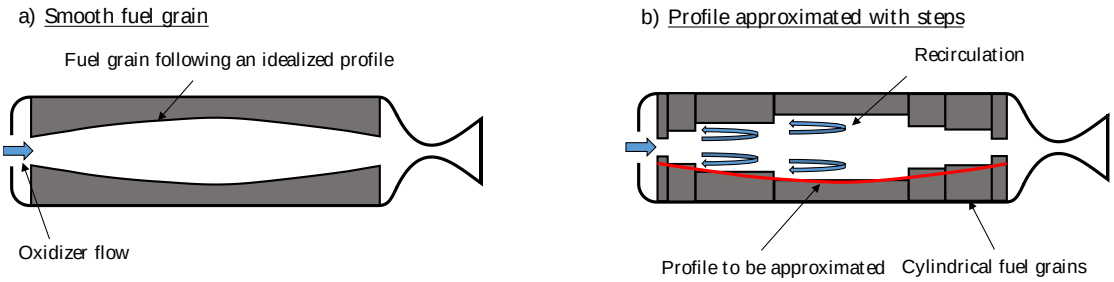

Figure 1: Approximation of fuel port profiles [12]

In the Ref. [12], several tests were carried out to study the influence of the BFS and FFS on the solid fuel regression rate on three different motors with different propellant couples. First, for the ULB-ATM HRE, a cylindrical motor using N_2O as oxidizer and HDPE as fuel, the theoretical positive effects of BFS and FFS grains were confirmed [12]. The FFS configuration increased the average solid fuel regression rate by 41.3 % above the reference trend line (single port); in the case of BFS, the increase was 15.7 %. Additional tests with the ULB-ATM *Mouette* slab burner (paraffin and oxygen) brought insights about the areas of higher regression rates through CH* intensity analysis. The 2D-slab burner campaign proved that a steps are also effective for paraffin grains in the two-dimensional domain [12].
In the following, another battery of tests employing the ONERA HYCAT motor was carried out. HYCAT uses H_2O_2 as oxidizer and HDPE as fuel. For HYCAT, the BFS case increased the average regression rate (+26.3 %), while the FFS had a negligible effect on the time and space averaged regression rate. This is in contrast to previous tests on the ULB-HRM engine, where FFS were more powerful. The explanation for this difference was not the different propellant couple but the total fuel grain length (and to a lesser extent the ratio of total fuel grain length to step height). Shorter grains benefit more from FFS, while longer grains profit from BFS [12].
To prove the concept of multiple steps as presented in Figure 1, Glaser et al. [13] tested multi-stepped fuel grains that also followed an optimized profile. The profiles were optimized using a genetic algorithm to decrease O/F shift and mixture ratios closer to stoichiometry. The overall regression rate could be increased by 80%, proving that multiple steps can be employed to cumulate the effect of steps. However, the optimization of the O/F could not be conclusively proven, most likely due to limited burn times [13].
In a follow up work, Glaser et al. [14], tested a novel grain configuration enabled by the stepped design approach named STEpped Helix HYbrid Rocket Engine (STEPHHY). The stepped helix approach is an evolution of the axial stepped profiles by taking the stepped approximation into the third dimension and allowing it to approximate a helical fuel port with steps. The results were positive with up to 245% regression rate increase. Moreover, the stepped helix design combines both a helical port and a stepped port, while considerably decreasing manufacturing complexity for helical fuel ports [14].
The present work complements the study of the stepped grains (optimized profile and stepped helix) by investigating the interaction between the pressure oscillation in the combustion chamber and the grain configuration on the HYCAT hybrid rocket motor. We are using a computation tool, named *WaVer*, developed at the University of Brasília Chemical Propulsion Laboratory, and apply the methodology proposed by Bertoldi et al. [7] and Lee et al. [15]. In Section 3, we present the approach adopted for this work.

1.1. Hybrid Rocket Instabilities

Hybrid rocket pressure oscillations of low frequency and large amplitude have been observed by many researchers [7, 15-17]. These oscillations are not as catastrophic for hybrid rocket engines as they are for liquid and solid systems. However, severe pressure oscillation can result in a significant reduction in the performance of the propulsion system, trigger other types of instabilities [16], or restrict the application of the technology, depending on mission requirements. The studies of available instability data suggest the existence of at least three major categories of hybrid combustion instability phenomena: (i) instability due to the time lag associated with vaporization and combustion of liquid droplets

DOI: 10.13009/EUCASS2023-514

(with liquid injection); ii) unstable burning associated with periodic accumulation and break-off of char layers or melted layers at the surface; (iii) the combustion instability mechanism similar to that encountered in solid propellants [18].

2. Experimental setup and fuel grain configurations

2.1 Experimental setup

The HYCAT (Hybrid with CATalyzer) motor uses H_2O_2 (87.5 %) and HDPE as propellants. The hydrogen peroxide is decomposed over a catalyst bed and injected into the combustion chamber. The oxidizer mass flow used for the tests is set to approximately 0.35 kg/s, measured with a Coriolis mass flow meter. Four piezoelectric pressure probes measure the chamber pressure in the pre- and post-chamber, and the temperature upstream of the axial injector is recorded as well. The length of the engine can be adjusted thanks to its modular design, allowing for a wide range of fuel grain lengths. The combustion gases are ejected through an ablatively cooled nozzle. In the presented tests, the engine was operated at around 25 bar chamber pressure leading to thrust ranges of around 700 N, which was measured with the thrust balance the engine is mounted on.

2.2 Fuel grain configurations and test conditions

With the aim to organize the discussion of the results, we separated the cases according to the grain geometry. First, we focus on the test with single BFS and FFS grains and the single circular port (baseline tests). Consequently, we investigate the multi-step configurations, and lastly the stepped helix fuel grains. Due to the characteristics of the HYCAT motor, the chamber pressure oscillations are coupled with the motor feed system. Apart from the solid fuel grain configuration, all other systems, and subsystems of the HYCAT motor were the same for all the data presented below.

2.2.1 Description of multi-stepped axial geometries

In a stepped case, the diameter before and after the step is different. Table 1 presents the main dimensions for the tests and Figure 2 shows the basic design of a BFS grain. For a FFS grain, D_1 is larger than D_2.

Table 1: Overview of the fuel grain main dimensions (single steps)

Test no.	Grain Configuration	D_1 (mm)	D_2 (mm)
H48	Single port	25	--
H49	Single port	40	--
H50	FFS	40	25
H51	BFS	25	40
H52	BFS	25	40

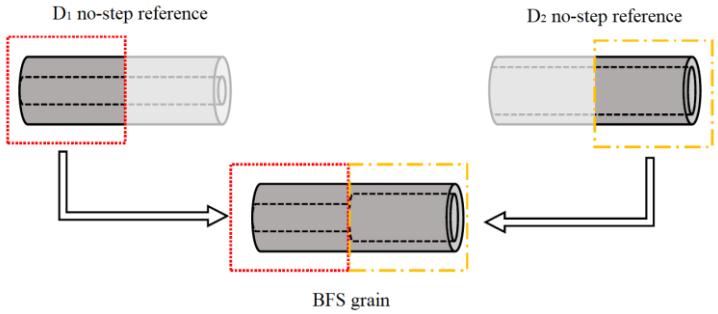

Figure 2: Visualization of BFS grain [12, with modifications]

For the concept of multiple steps, different segments or slices with different inner diameters (or any other desired geometric characteristic) are assembled together so that they represent an optimized fuel grain geometry that is

DOI: 10.13009/EUCASS2023-514

approximated by steps [13]. The details of the optimization process are not elaborated in this work but can be found in Ref. [13].
The influence of the multi-step grains on the combustion chamber pressure oscillations is analysed with data from tests H55, H56, H57 and H60. The number of grain segments, steps and step heights are listed in Table 2. Figure 3 illustrates the assembled H56 grain after the test.

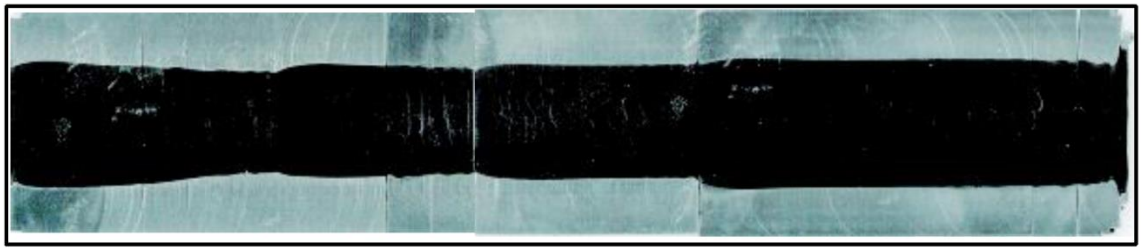

Figure 3: H56 profile after test [13]

2.2.2 Description of stepped helix (STEPHHY)

The helical design consists of a series of solid fuel grain segments that are rotated against each other to form a stepped helical fuel port [14]. Due to the rotation of each slice, a helical structure with steps is introduced that forces the oxidizer flow into a swirling motion. Figure 4 presents the initial STEPHHY I concept, and Figure 5 shows the STEPHHY X (or CROSS because of the cross-section fuel port). Detailed information about the design and propulsive performance of the helical grain is available in Glaser et al. [14]. Table 2 summarises the main dimensions of multi-step tests and STEPHHY.

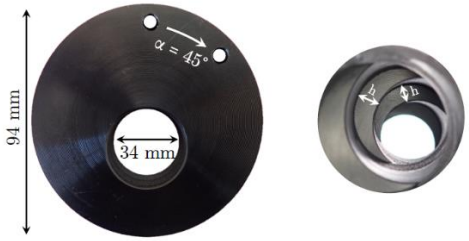

Figure 4: One segment of initial STEPHHY I [14]

Figure 5: Port design of STEPHHY X [14]

Table 2: Overview of the fuel grain configurations (multiple segments) [13,14]

Test no.	Grain Configuration	Step height, (mm) / step configuration	grain segments
H55	Multi-step	7.5 (3 x FFS) – 7.5 (4 x BFS)	8
H56	Multi-step	2 (7 x FFS) – 4 (3 x BFS)	11
H57	Multi-step	8 (2 x FFS) – 4 (4 x BFS)	7
H58	STEPHHY I	7.65 – 7.85	17
H59	STEPHHY X	4.29 – 4.32	10
H60	Multi-step	4 (4 x FFS) – 8 (2 x BFS)	7

DOI: 10.13009/EUCASS2023-514

3. Frequency Analysis

To study the pressure oscillations in the combustion chamber, two pressure probes in the post-chamber with a sample rate of 5 kHz are used. The other pressures acquired were the pressure in the catalytic bed (two sensors), pressure in the feed lines, such as before the oxidizer valve and in the hydrogen peroxide tank.
Through analysis of the pressure signal obtained from the combustion chamber, it becomes evident that small amplitude oscillations occur during the combustion process. This is because in the HYCAT tests the chamber pressure is not isolated from other critical motor subsystems, such as the oxidizer lines and oxidizer tank. This lack of isolation leads to a significant influence of low-frequency chamber pressure oscillations and complex interactions with the feed system. The interplay between these factors can result in undesirable pressure fluctuations within the combustor.
It is worth highlighting that feed-system coupled instabilities exhibit distinct characteristics compared to TCG (Thermal-Combustion-Gasdynamic) coupled instabilities that primarily originate from the boundary layer response time. In the case of feed system instabilities, the dominant frequencies strongly correlate with the residence time of gases within the post-chamber and the inherent flow characteristics. In-depth analysis of the experimental data allows for the identification of specific conditions in which hybrid rocket motors demonstrate reduced combustion instabilities associated with the (liquid) oxidizer feed system [15, 19, 20].
To start the frequency analysis, the raw data is imported into the *WaVer* program and the dataset of interest is chosen (Figure 6). The *WaVer* is a Python-based tool developed at the University of Brasília Chemical Propulsion Laboratory (UnB/CPL) and the main advantage is that the program is user-friendly, flexible and allows manipulating the data without needing to rewrite the code to adjust to the user requirements, thus, all the analysis can be performed in the same program. The code performs the DFT (Discrete Fourier Transform) of the signal by an FFT (Fast Fourier Transform) algorithm (Figure 7) and presents the SFT (Short-Time Fourier Transform) in both 2D and 3D spectrograms (Figure 8). Figure 9 presents the spectral density, and mathematically it is defined as the Fourier transform of the autocorrelation sequence of a time series, which is obtained by performing a Fourier transform on the autocorrelation function. The spectral density represents the average squared magnitudes of the Fourier transforms, or in a simple way, it describes the frequency content of a signal and can be utilized to detect periodic patterns in the data, such as time variation of the combustion chamber pressure. By examining peaks at frequencies corresponding to these periodicities, it is possible to identify and analyse the presence of such patterns. Reference [21] defines the spectral density function with mathematical formalism and discusses the properties of the spectral density estimation, and reference [22] presents an overview about the estimation of the spectral density using DFT/FFT.
Data results from the firing test, together with calculated stability parameters are given in Table 3. ΔP is the injector pressure drop measured as the difference between the feed line pressure near the oxidizer main valve and the chamber pressure. The parameter P'_{max}/P_c is the maximum initial chamber pressure oscillation amplitude divided by the initial chamber pressure and it is commonly used to quantify chamber pressure oscillations.

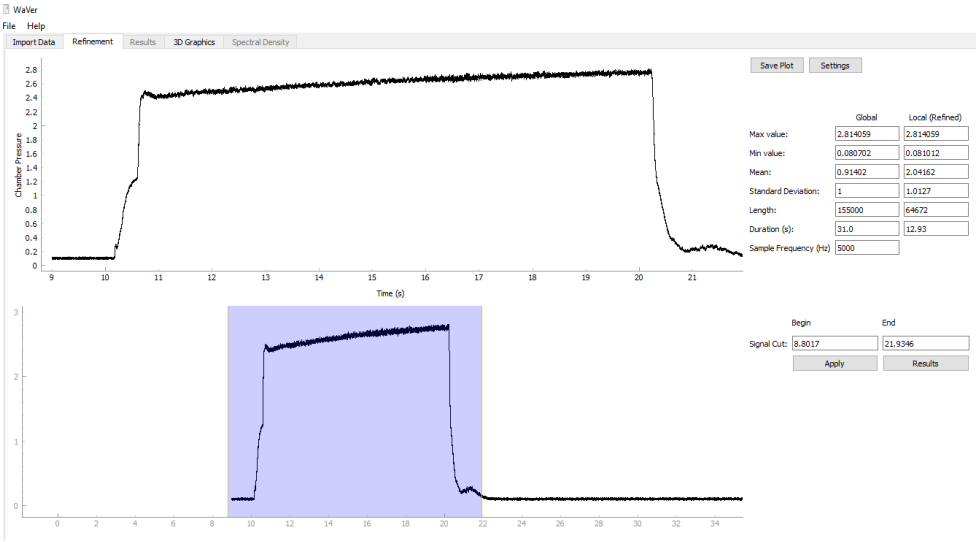

Figure 6: Data refined, test H48

For the analysis, the initial values are the experimental parameters. The initial geometry of the combustion chamber is based on the initial fuel port diameter and length, the initial volumes of the combustion chamber, the injector cavity, and the post-combustion chamber. However, the grain geometry is consumed over the burn time, which changes the

DOI: 10.13009/EUCASS2023-514

internal geometry. This indicates a limitation of the methodology to estimate pressure oscillations [7, 15]. The implications of this will be discussed later in this paper.
The initial fundamental frequency, f_{ini}, was taken at the onset of combustion instabilities. As the injector plate, catalytic bed length, and injector cavity were kept constant during all the tests, we assume that the oxidizer properties at the entrance of the fuel combustion port were roughly the same throughout the test campaigns. This remark is important because the size of the injector cavity has a major impact on the feed-system coupled instability.

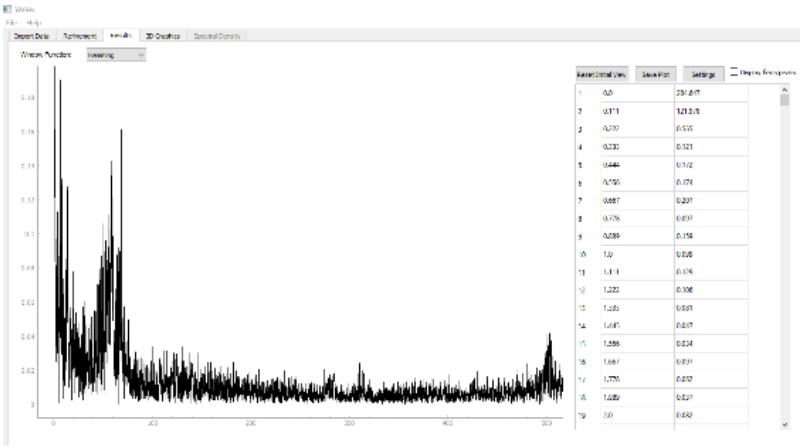

Figure 7: DTF, test 48

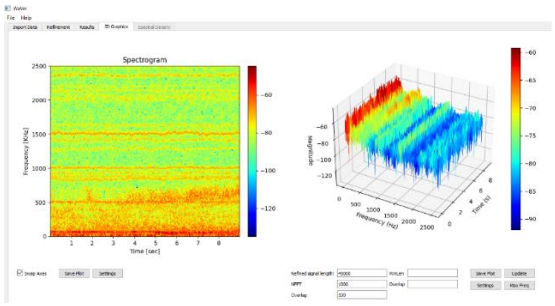

Figure 8: Results of the STF, test H48

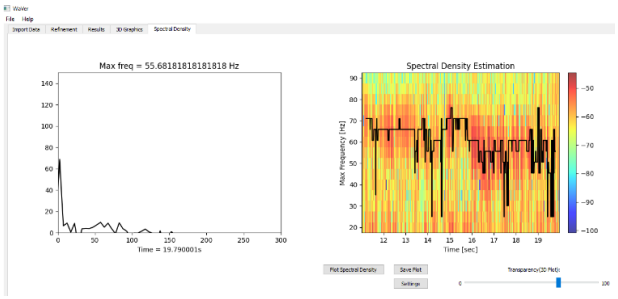

Figure 9: Estimation of the spectral density, test H48

Figure 10 presents the chamber dynamic pressure plots of H48 and Figure 11 the Fourier transform of the same test. The combustion process took place at an average chamber pressure of 26 bar with an injector pressure drop (difference between the feed line pressure near the oxidizer main valve and the chamber pressure) of 15 bar. The Fourier transform indicates that the fundamental frequency spans from about 50 Hz to 500 Hz, which differs from liquid rocket engines since pressure signals in liquid engines occur in a narrow bandwidth [15].
The fundamental frequency of the combustion chamber is presented in Figure 12 for test H48 and Figure 13 for test H51. The same study was carried out for all the tests and the main findings are presented in the next section.

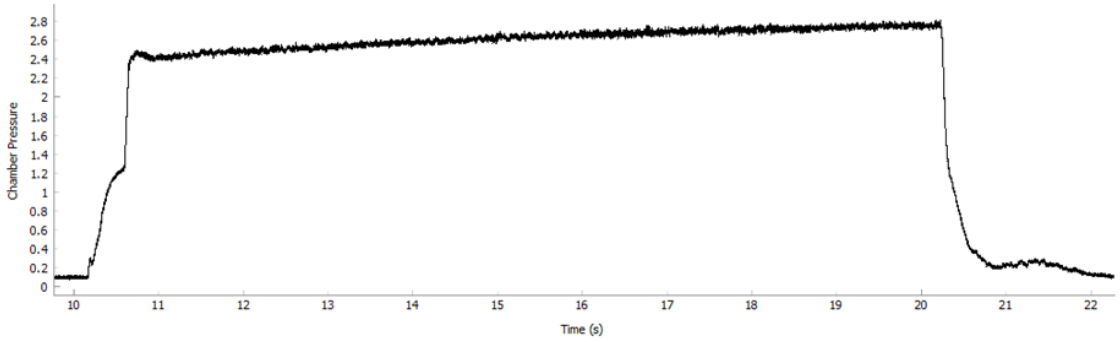

Figure 10: Test H48 chamber dynamic pressure (MPa)

DOI: 10.13009/EUCASS2023-514

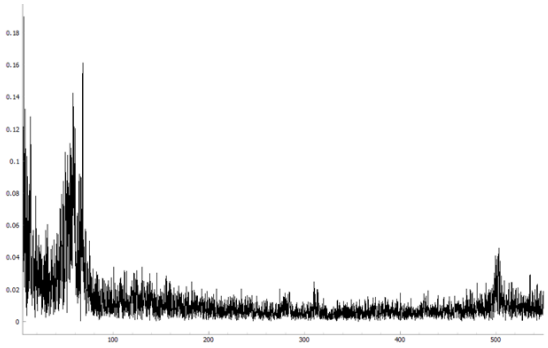

Figure 11: Test H48 Fourier transform

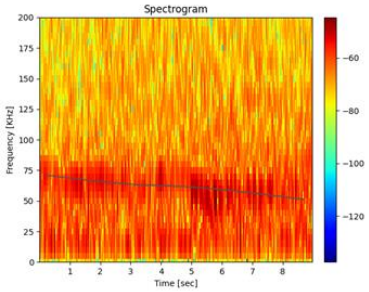

Figure 12: Contour plots of Fourier transform in time-frequency for test H48

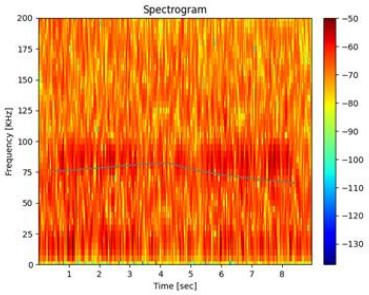

Figure 13: Contour plots of Fourier transform in time-frequency for test H51

Table 3: HYCAT chamber pressure oscillations results

Test no.	**Fuel grain**	$\bar{D}_0, mm$	$\bar{P}_c, bar$	$\Delta P, bar$	P'_{max}/P_c, %	f_{ini}, Hz
H48	Single port	25	26,25	15.11	15.51	71.02
H49	Single port	40	24.21	13.70	8.63	45.45
H50	FFS	32.5	25.46	11.93	9.09	50.56
H51	BFS	32.5	27.19	11.54	2.99	60.79
H52	BFS	32.5	28.36	9.00	5.74	40.34
H55	Multi-steps	34	27,99	8.56	6.61	35.23
H56	Multi-steps	40.1	25,96	11.80	4.37	35.22
H57	Multi-steps	40.4	27.03	10.19	3.82	35.23
H60	Multi-steps	40.4	27.33	10.30	2.56	30.11

DOI: 10.13009/EUCASS2023-514

4. Discussion of the Results

For better overview, we separate the discussion of results into the axial stepped profiles (H50-H52, H55-H57 & H60) and the stepped helix tests (H58&H59).

4.1. Results for multi-stepped axial fuel grains

Figures 14, 15, and 16 present the spectrogram for the stepped grain tests H50 (single FFS), H55, and H56 (both multi-stepped), respectively. Let us compare the contour plots of the Fourier transform in time frequency for the tests H48 (no step reference) and H51 (single BFS) in Figures 12 & 13 with the plot of the tests H50 (single FFS), H55, and H56 (both multi-stepped) in Figs. 14-16. It is possible to note that the fundamental oscillation frequency for H48 & H51 does not shift significantly over time, while for the tests H50, H55, and H56 it is not possible to determine any trend. This result is likely because of the unique shape of the fuel grains developed. For test H48 the grain port configuration is a single cylinder as in most of the experiments with HREs, and the behaviour shown in Figure 12 is the same as found by Lee et al. [15] for the same fuel but using nitrous oxide as oxidizer. It seems that the same behaviour is true for the test H51 (BFS type). Both grains in these cases have a combustion port of 25 mm in the first half, with the main difference being that for test H51 (BFS grain) the port diameter in the second grain half increases to 40 mm (Figure 2).
When we compare the real-time estimation of the spectral density for the tests H48 and H51, in Figure 17 and Figure 18, respectively, it is possible to note that the initial frequencies are close, between 60.79 – 71.02 Hz. For test H51, the trend of the plot (Figure 18) indicates a slight increase in the frequency, from the initial value of 60 Hz to around 80 – 90 Hz, after 16 *s*. For test H48, the behaviour is the opposite, because the frequencies tend do decrease with time. The behaviour of decreasing frequency of the unstable test (H48) agrees with references [7, 20].

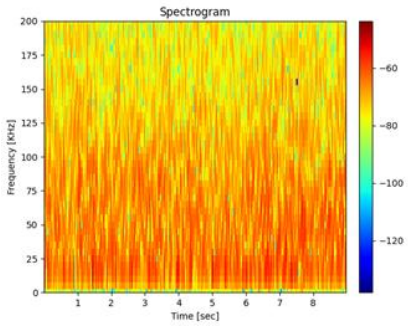

Figure 14: spectrogram for the test H50

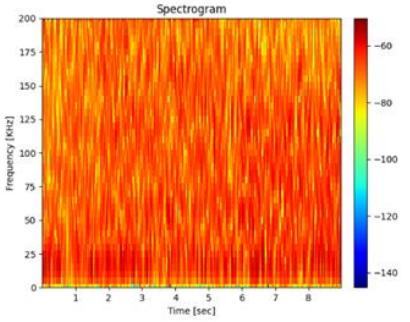

Figure 15: spectrogram for the test H55

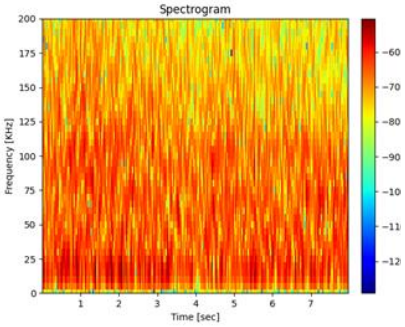

Figure 16: spectrogram for the test H56

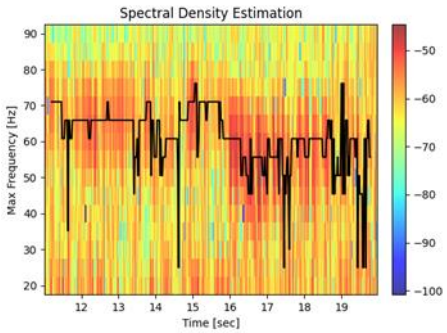

Figure 17: Spectral density for test H48

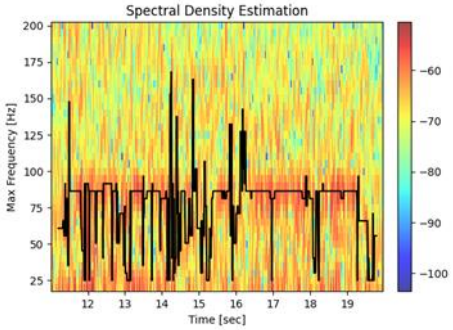

Figure 18: Spectral density for test H51

In the test H50, which uses a single FFS grain, the maximum amplitude of the oscillations is 9.1% with an initial frequency of 50.6 Hz. In general, the maximum frequency for the FFS grain is still lower than for the BFS configuration (H51), and close to a single port configuration. It is to be noted here, that the BFS oscillations (H51 & H52) are lower than the FFS oscillations (H50). Lee et al. [23] have already shown that BFS can decrease pressure oscillations. Figure 19 presents the maximum frequency of the real-time estimation of the spectral density for test H50.
The test H56 (multi-stepped grain) presents a very stable pattern with a maximum amplitude of oscillation less than 5 % (usually accepted as stability limit) and Figure 21 shows that the maximum frequency of the real-time estimation of

DOI: 10.13009/EUCASS2023-514

the spectral density is smoother in comparison with test H55 (Figure 20). Both test H55 and test H56 have multiple steps; however, test H56 has a smaller step height (2 - 4 mm) and more grain segments (11) than test H55 (7.5 mm step height and seven segments). This indicates that the height of the steps has a more important impact on the chamber oscillations than the number of steps.
The impact of the type of step on the oscillations can best be shown when comparing test H57 with H60. Test H57 is a multi-step test with two FFS with 8 mm height and four BFS with a step height of 4 mm, while test H60 has four FFS steps with 4 mm height followed by two BFS with height of 8 mm [13]. Both tests have similar average chamber pressure (~ 27 bar) and pressure drop (~10 bar), and the average maximum chamber pressure oscillations are 3.82 % for test H57, and 2.56 % for test H60. Figure 22 shows the maximum frequency of the real-time estimation of the spectral density for test H57, and Figure 23 presents the same information for test H60, where it is possible to derive that the distribution of the maximum frequency for test H60 is more uniform in comparison with test H57, therefore more stable. It is important to note that for both tests, H57 and H60, the maximum pressure oscillation was less than 5%. We can observe another important characteristic here: Lee at al. [21] have shown that BFS can decrease pressure oscillations, while diaphragms (which can be loosely interpreted as FFS) increase the pressure oscillations. This could explain why H60 is more stable than H57, given that H57 has higher FFS (8 mm) and smaller BFS (4 mm) and H60 has higher BFS (8 mm) and smaller FFS (4 mm).

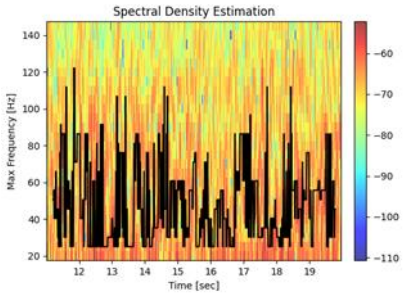

Figure 19: Spectral density for test H50

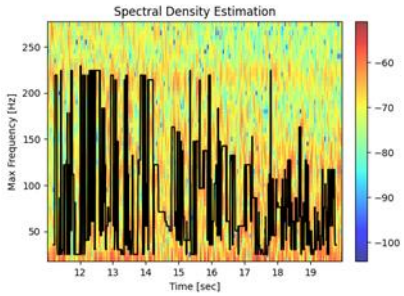

Figure 20: Spectral density for test H55

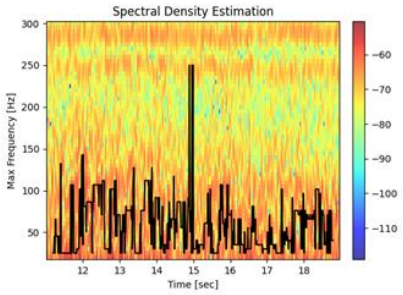

Figure 21: Spectral density for test H56

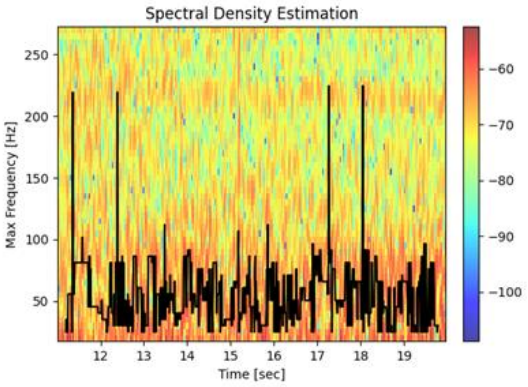

Figure 22: Spectral density for test H57

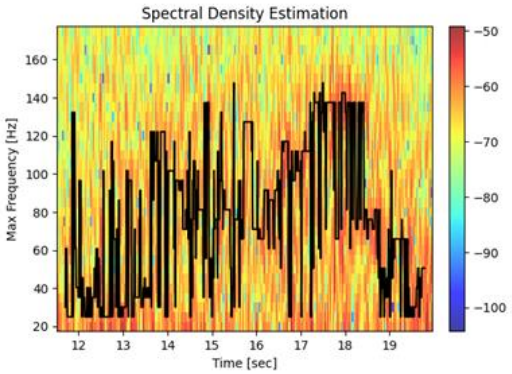

Figure 23: Spectral density for test H60

4.2. Results for stepped helix (STEPHHY)

Let us now change the attention from the axial stepped grains to the stepped helix grains [14]. Table 4 presents the frequency analysis of the STEPHHY tests. The configuration of the STEPHHY I grains can be seen in Figure 4 while Figure 5 shows the STEPHHY X concept. The average pressure for test H59 is slightly lower than for test H58, but the pressure drop between the chamber and the feed system is similar. As defined before, the parameter P'_{max}/P_c is the maximum initial chamber pressure oscillation amplitude divided by the initial chamber pressure and it is commonly used to quantify chamber pressure oscillations.
The value for P'_{max}/P_c of test H58 is almost 11 % and close to the tests with the single port configuration (H48 and H49) and FFS grain (H51). The oscillations of pressure for STEPHHY X (test H59) are inside the stability criteria, but the value of 2.47 % (*) is to be regarded with caution. The pressure in the chamber continuously decreases during the engine operation due to nozzle erosion (the nozzle throat diameter eroded from 16 mm to 16.9 mm). Moreover, the regression rate shifted considerably over time due to the design choices of STEPHHY X [14]. Figure 24 shows the

DOI: 10.13009/EUCASS2023-514

maximum frequency of the spectral density for test H58, and Figure 25 presents the same information for the test H59. It is likely that the significant increase of the maximum pressure density for test H59 (Figure 25) at around 11.5 seconds is caused by the changing of the geometry of the combustion port over time and the nozzle erosion.

Table 4: HYCAT chamber pressure oscillations result for Helix grains

Test no.	**Fuel grain**	$D_0(mm)$	$\overline{P}_c, bar$	$\Delta P, bar$	P'_{max}/P_c, %	f_{ini}, Hz
H58	STEPHHY I	34.00	28.68	9.38	10.85	35.23
H59	STEPHHY X	22.24	26.88	9.19	2.47*	30.11

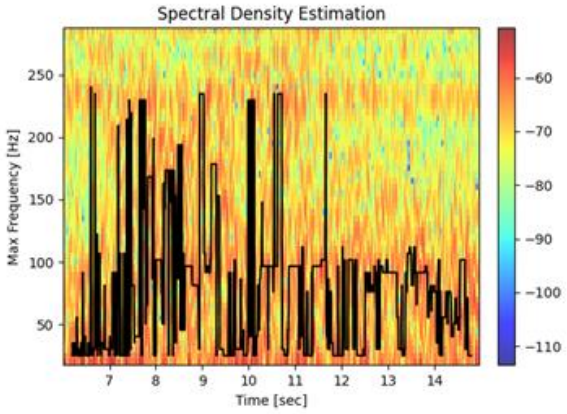

Figure 24: Estimation of the spectral density, test H58

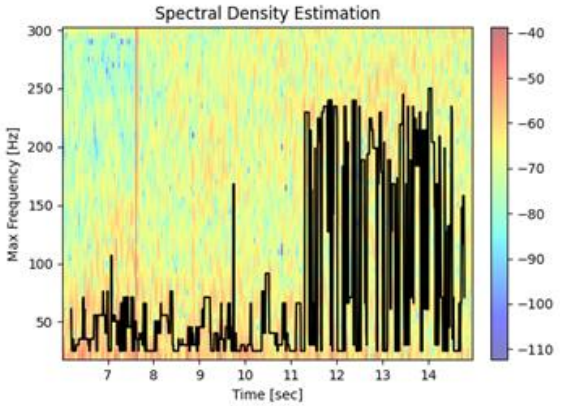

Figure 25: Estimation of the spectral density, test H59

4. Conclusion and Final Remarks

Hybrid rocket motors have been experiencing combustion instability phenomena in various projects at different motor sizes. The feed-system coupled instability is a type of dynamic instability in which the time-dependent response of the propellant flow is related to the unsteady combustion pressure. The intrinsic low-frequency instability is caused by the coupling of the thermal lags, the gas-phase combustion, and the gas dynamic subsystems of the hybrid rocket.
The maximum frequency (peak) of the spectral density for all tests was lower than 300 Hz, consistent with the intrinsic low frequency of the hybrid rocket motors, but also influenced by the feed-system coupled instabilities. However, the HYCAT engine uses a catalytic bed and injector cavity, which increase the distance between oxidizer entrance and the front of the fuel grain port, those lengths (L) impact the fundamental frequency, $f \propto 1/L^{0.6}$ [15]. As, in this specific

DOI: 10.13009/EUCASS2023-514

study, the length of both the catalytic bed and cavity were the same for all the tests presented, we consider that this condition affected all experiments equally, thus, it is not the principal reference parameter for the pressure oscillation. The main purpose of this study was to investigate the impact of grain geometry on the pressure oscillations in the combustion chamber. More precisely, we investigated how steps in the fuel grains affect the combustion behaviour. First, we used a single circular combustion port, as a reference, and it was possible to note pressure oscillations in the combustion chamber around 15.5 % and 8.7 %, which is higher than 5%, which commonly adopted as the upper stability limit. For the test H50 (single FFS) the values of the pressure oscillations were close to the reference case. These findings are following the trend of the ballistic behaviour of the motor, because the FFS had a negligible effect on the average regression rate on the HYCAT engine [12].

In the case of multi-step tests, the average regression rate is very close for all the cases, between 0.5 mm/s and 0.8 mm/s, like the values for the references (H48 & H49) and single FFS and BFS cases. For H55 with larger FFS heights, we observed pressure oscillations of 6.6 %. For test H56, we observed pressure oscillations of around 4.4%, for a configuration with 11 segments (out of which 7 steps are FFS), however with a smaller step height (2-4 mm). It seems that the size of the FFS grains have a bigger impact on the oscillatory behaviour of the combustion chamber process than the number of steps. If we compare tests H57 and H60, the impact of the step type becomes apparent. Test H57 has large FFS (8 mm) and small BFS (4 mm). On the other hand, H60 has large BFS (8 mm) and small FFS (4 mm). In our analysis, H60 (2.56 %) is more stable than H57 (3.82 %), which leads to the conclusion that BFS increase the stability more than FFS. The positive impact of BFS on pressure oscillations in HREs has already been reported in the literature [23].

For the stepped helix designs (STEPHHY), the overall regression rate was significantly higher due to the new design (up to +245% compared to the reference). Quantitatively speaking, for the tests H58 (STEPHHY I) and H59 (STEPHHY X), the regression rates were 1.18 mm/s and 1.49 mm/s, respectively. However, the signal of the pressure in the combustion chamber differs drastically in both cases. STEPHHY I (H58) had high frequencies at the beginning of the burn (Figure 24) and that shifted to lower values over time. STEPHHY X (H59) shows a very stable behaviour at the begging of the test because the variation (maximum and minimum) of frequency estimated by the spectral density (peaks) varies between 30 Hz and less than 100 Hz from the beginning of the test, until the time 11 *s* (approximately). After, the time 12 *s* (approximately) the estimation of the frequencies changing quick and continuous from around 50 Hz to about 250 Hz. If we compare P'_{max}/P_c, it is smaller for test H59 in comparison with the test H58. The interpretation of the results for the stepped helix is more delicate. This is due to the particularities of the stepped helix design, where the initial helical port of the helix (most pronounced for H59) is "weakened" over time because of the progression of the fuel port. This leads to a shift in regression rate over time, with a fast-changing inner geometry [14]. The interdependency of pressure oscillations, multi-step helical ports with fast changing geometries and pronounced regression rate shift is not yet fully understood and subject for future investigations.

Summarizing, we have shown that steps have a non-negligible (mostly positive) impact on the pressure oscillations of HREs. The step height is more significant than the number of steps, and the type of step is the most important characteristic. BFS have a more stabilizing effect on the chamber pressure than FFS. Nonetheless, we like to stress that none of the multi-stepped and stepped helix cases exhibited pressure oscillations that were higher than the most unstable reference case without step, although all the multistep grains and the helical design showed significantly higher regression rates.

Acknowledgments

The project leading to this application has received funding from the European Union's Horizon 2020 research and innovation programme under the Marie Sklodowska-Curie grant agreement No 860956. It is part of the ASCenSIon project, an Innovative Training Network (ITN) to advance space access capabilities (https://ascension-itn.eu/).

A. E. M. Bertoldi received funding from the Marie Sklodowska-Curie grant agreement No 801505.

References

[1] Mazetti, A., Merotto, L., Pinarello, G. 2016. Paraffin-based Hybrid Rocket Engines Applications: A Review and a Market Perspective. *Acta Astronautica*, vol. 126

[2] Okninski, A., Kopacz, W., Kaniewski, D., Sobczak, K. 2021. Hybrid Rocket Propulsion Technology For Space Transportation Revisited – Propellant Solutions and Challenges. *FirePhysChem*

[3] Bouziane, M., Bertoldi, A.E.M., Milova, P., Hendrick, P., Lefebvre, M. 2019. Performance comparison of oxidizer injectors in a 1-kN paraffin-fueled hybrid rocket motor. *Aerospace Science and Technology*, 89: 392-406.

[4] Humble, R. W., Henry, G. N., Larson, W. J.1995. Space Propulsion Analysis and Design. Space Technology Series, McGraw-Hill.

DOI: 10.13009/EUCASS2023-514

[5] Casalino, L., Pastrone, D. 2010. Optimal Design of Hybrid Rocket Motors for Launchers Upper Stages. *Journal of Propulsion and Power*, vol. 26, No. 3.
[6] Karabeyoglu, A., Zilliac, G., Cantwell, B., Dezilwa, S., Castellucci, P. 2004. Scale-up Tests of High Regression Rate Paraffin-Based Hybrid Rocket Fuels. *Journal of Propulsion and Power*, 20: 1037-1045.
[7] Bertoldi, A. E. M., Bouziane, M., Lee, J., Veras, C. A. G., Hendrick, P., Simone D. 2019. Theoretical and Experimental Study of Combustion Instability in Hybrid Rocket Motors. In: *8th European Conference for Aeronautics and Space Sciences (EUCASS)*. Madrid, Spain.
[8] Oztan, C., Ginzburg, E., Akin, M., Zhou, Y., Leblanc, R.M., Coverstone, V. 2021. 3D printed ABS/paraffin hybrid rocket fuels with carbon dots for superior combustion performance. *Combustion and Flame*. 225: 428-434.
[9] Zhang, S., Hu, F., Zhang, W. 2016. Numerical Investigation on the regression rate of Hybrid Rocket Motor with Star Swirl Fuel Grain. *Acta Astronautica*, 127: 384-393.
[10] Nguyen, C., Thomas, J. C. 2023. Performance of Additively Manufactured Fuels for Hybrid Rockets. *Aerospace*, 10(6).
[11] Glaser, C., Hijlkema, J., Anthoine, J. 2022. Evaluation of Regression Rate Enhancing Concepts and Techniques for Hybrid Rocket Engines. *Aerotecnica Missili & Spazio*
[12] Glaser, C., Gelain, R., Bertoldi, A. E. M., Levard, Q., Hijlkema, J., Lestrade, J.-Y., Hendrick, P., Anthoine, J. 2023. Experimental Regression Rate Profiles of Stepped Fuel Grains in Hybrid Rocket Engines *Acta Astronautica*, 204.
[13] Glaser, C., Hijlkema, J., Lestrade, J.-Y., Anthoine, J. 2023. Hybrid Rocket Engines Optimized by Multi-Stepped Design Approach: Experimental Investigation. In: *The 34th International Symposium on Space Technology and Science, Kurume, Japan*.
[14] Glaser, C., Hijlkema, J., Lestrade, J.-Y., Anthoine, J. 2023. The Stepped Helix Hybrid Rocket Engine. In: *AIAA AVIATION Forum*, San Diego, USA.
[15] Lee, J., Bertoldi, A.E.M., Andrianov, A., Borges, R.A., Veras, C.A.G., Battistini, S., Morita, T., Hendrick, P. 2020. Role of Precombustion Chamber Design in Feed-System Coupled Instabilities of Hybrid Rockets. *Journal of Propulsion and Power*. 36(6):1-10.
[16] Karabeyoglu, A., Zilliac, G., Cantwell, B. J., De Zilwa, S., and Castellucci, P. 2004. Scale-Up Tests of High Regression Rate Paraffin-Based Hybrid Rocket Fuels. *Journal of Propulsion and Power*. 20(6): 1037–1045.
[17] Park, K. S., and Lee, C. 2015. Low Frequency Instability in Laboratory - Scale Hybrid Rocket Motors. *Aerospace Science and Technology*. 42: 148–157.
[18] National Aeronautics and Space Administration- NASA.1969. Investigation of Combustion Instability in Hybrid Rockets. Report: *NASA CR-66812. SRI*. Langley Research Centre (USA).
[19] Karabeyoglu, A., De Zilwa, S., Cantwell, B., Zilliac, G. 2005. Modeling of Hybrid Rocket Low Frequency Instabilities. *Journal of Propulsion and Power*. 21(6): 1107–1116.
[20] Bertoldi, A.E.M., Bouziane, M., Veras, C.A.G., Lee, J., Costa, M.V.C. 2018. Experimental Investigation of the Feed System Instabilities in Hybrid Rocket Motors. In: 69th International Astronautical Congress, Bremen, Germany.
[21] Wirsching, P.H., Paez T., Ortiz K. Random Vibrations, Theory and Practice.1995. Dover publications Inc.
[22] Heinzel, G., Rudiger, A., Schilling, R. 2002. Spectrum and spectral density estimation by the Discrete Fourier transform (DFT), including a comprehensive list of window functions and some new flat-top windows. Report. Max-Planck-Institut fur Gravitationsphysik, Albert-Einstein-Institut. 84 pages.
[23] Lee, J., Rhee, S., Kim, J., Moon, H. 2021. Combustion Instability Mechanism in Hybrid Rocket Motors with Diaphragm. Journal of Propulsion and Power